RELATIONSHIP BETWEEN AEROSOL OPTICAL DEPTH AND PARTICULATE MATTER OVER SINGAPORE: EFFECTS OF AEROSOL VERTICAL DISTRIBUTIONS

Boon Ning CHEW[1], James R. CAMPBELL[2], Edward J. HYER[2], Santo V. SALINAS[1], Jeffrey S. REID[2], Ellsworth J. WELTON[3], Brent N. HOLBEN[4] and Soo Chin LIEW[1]

[1]Centre for Remote Imaging, Sensing and Processing, National University of Singapore, Block S17, Level 2, 10 Lower Kent Ridge Road, Singapore 119076
[2]Naval Research Laboratory, Marine Meteorology Division, 7 Grace Hopper Avenue Stop 2, Monterey, CA USA 93943-5502
[3]Micro-Pulse Lidar Network, Code 613.1, NASA Goddard Space Flight Center, Greenbelt, MD 20771 USA
[4]Code 618, NASA Goddard Space Flight Center, Greenbelt, MD 20771 USA

Corresponding author: Boon Ning CHEW
Email: Chew_Boon_Ning@nea.gov.sg
Tel: +65 64881857
Fax: +65 62899313

ABSTRACT

As part of the Seven Southeast Asian Studies (7SEAS) program, an Aerosol Robotic Network (AERONET) sun photometer and a Micro-Pulse Lidar Network (MPLNET) instrument have been deployed at Singapore to study the regional aerosol environment of the Maritime Continent (MC). In addition, the Navy Aerosol Analysis and Prediction System (NAAPS) is used to model aerosol transport over the region. From 24 September 2009 to 31 March 2011, the relationships between ground-, satellite- and model-based aerosol optical depth (AOD) and particulate matter with aerodynamic equivalent diameters less than 2.5 μm ($PM_{2.5}$) for air quality applications are investigated. When MPLNET-derived aerosol scale heights are applied to normalize AOD for comparison with surface $PM_{2.5}$ data, the empirical relationships are shown to improve with an increased 11 %, 10 % and 5 % in explained variances, for AERONET, MODIS and NAAPS respectively. The ratios of root mean square errors to standard deviations for the relationships also show corresponding improvements of 8 %, 6 % and 2 %. Aerosol scale heights are observed to be bimodal with a mode below and another above the strongly-capped/deep near-surface layer (SCD; 0 – 1.35 km). Aerosol extinctions within SCD are well-correlated with surface $PM_{2.5}$ concentrations, possibly due to strong vertical mixing in the region.

Keywords: Air Pollution, Air Quality, Aerosol Optical Depth

1 INTRODUCTION

In the form of respirable particulate matter with aerodynamic equivalent diameter of less than 10 μm (PM_{10}) and 2.5 μm ($PM_{2.5}$), atmospheric aerosol particles pose a significant public health risk. Common health implications include cardiopulmonary conditions, acute and chronic respiratory infections, and lung cancer (Cohen et al., 2005). In response to worsening regional air pollution in Southeast Asia (SEA) and the Maritime Continent (MC), due to increased industrial and urban emissions (e.g., Salinas et al., 2009; Reid et al., 2013), as well as regional biomass burning smoke (e.g., See et al., 2006, 2007; Salinas et al., 2013a, 2013b) from land preparation and forest clearing activities (e.g., Field et al., 2009), several ground-based air quality monitoring networks, such as those operated by Malaysia's Department of Environment (DOE; http://apims.doe.gov.my), Singapore's National Environment Agency (NEA; http://www.nea.gov.sg) and Thailand's Pollution Control Department (PCD; http://www.pcd.go.th), have been established. These networks provide information on air quality, including mass concentrations for PM, carbon monoxide, nitrogen oxide, sulphur dioxide and ozone, which serves as the basis for issuing public health advisories in cases of deteriorating air quality. While such networks are suitable for assessing air pollution from local sources, they are relatively limited spatially, and have poor representativeness of the vast rural areas in the region. Therefore, satellite-based remote sensing observations (e.g. Hoff and Christopher, 2009) and aerosol transport models (e.g., Hyer and Chew, 2010; Wang et al., 2013; Kim et al., 2014) with wide spatial coverage can be used to complement the operations of air quality monitoring networks, and provide needed information on the spatial distribution of regional air pollution, especially in cases of significant biomass burning outbreak (e.g., Reid et al., 2013).

Chu et al. (2003), as well as Wang and Christopher (2003), first demonstrated the capabilities of the Moderate Resolution Imaging Spectroradiometer (MODIS; Remer et al., 2005)

on board the National Aeronautics and Space Administration's (NASA) Terra and Aqua satellites to correlate satellite-based aerosol optical depth (AOD) with surface PM_{10} and $PM_{2.5}$ measurements respectively. Liu et al. (2004; 2005) also showed the Multi-Angle Imaging Spectroradiometer (MISR; Diner et al., 2002) on board Terra to have similar capabilities for air quality applications. Several research efforts have worked towards establishing empirical satellite-based AOD-PM relationships in different regions of the world (e.g., Engel-Cox et al., 2004b; Gupta et al., 2006; Schaap et al., 2008), as well as deriving satellite-based AOD products with higher resolution for comparison to urban domains (e.g., Li et al., 2005; Kumar et al., 2007; Wong et al., 2011; Bilal et al., 2013). Meteorological parameters, such as relative humidity (RH), wind direction and speed (e.g., Gupta and Christopher, 2009a, 2009b), are also shown to be important in establishing AOD-PM correlations.

There are certainly large-scale relationships between ambient columnar integrated AOD and surface PM concentration, but beyond this, the variability in aerosol vertical distribution and particle hygroscopicity lead to significant regional variability between the two parameters (Toth et al., 2014). Although Engel-Cox et al. (2006) has qualitatively demonstrated the potential of lidar-derived aerosol vertical distribution to constrain the AOD-PM relationship, the increasing availability of continuous long-term global ground-based lidar measurements provides the necessary data to assess the quantitative impact (Tsai et al., 2011; Chu et al., 2013). Given the complex meteorological environment of SEA and the MC, such an analysis requires the incorporation of continuous long-term lidar measurements over many seasons to limit inter-annual variance (Campbell et al., 2013; Reid et al., 2012, 2013).

Singapore Aerosol Robotic Network (AERONET; Holben et al., 1998) and Micro-Pulse Lidar Network (MPLNET; Welton et al., 2001) datasets have previously been considered in tandem for quantifying and characterizing the seasonal variability of aerosol particle columnar optical

properties and vertical distributions at the National University of Singapore (NUS) atmospheric measurement supersite from 24 September 2009 to 31 March 2011 (Chew et al., 2013). In this study, modified aerosol scale heights (Hayasaka et al., 2007) are derived from vertically-resolved MPLNET AOD profiles, and used to evaluate AERONET, MODIS and Navy Aerosol Analysis and Prediction System (NAAPS; Witek et al., 2007; Reid et al., 2009; Westphal et al., 2009) modeled AOD-$PM_{2.5}$ relationships over Singapore for the same study period. Over Singapore, transported aerosol layers within the residual boundary layer may be mixed into the surface layer by way of the entrainment zone (Atwood et al., 2013). This mechanism might complicate the development of any AOD-$PM_{2.5}$ (empirical or otherwise) correlations. The correlations will also likely be affected by varying aerosol hygroscopic growth coupled with high RH, resulting in yet more variable light scattering efficiencies in ambient conditions (Salinas et al., 2013a; 2013b).

In this paper, we describe a study to investigate the extent to which satellite, ground based and model simulated AOD relates surface PM in Singapore from 24 September 2009 to 31 March 2011. This is conducted with the aid of the aforementioned MPLNET instrument to help interpret aerosol vertical distributions. The modified aerosol scale heights (e.g., Hayasaka et al., 2007) is derived from MPLNET data, and used to normalize AOD in order to estimate the hourly surface $PM_{2.5}$ concentrations. A simple hygroscopic growth correction based on the assumption of a sulfate environment in Singapore (See et al., 2006) is also applied to minimize the differences between ambient $PM_{2.5}$ concentrations and the measured $PM_{2.5}$ dry mass. Finally, in order to evaluate the models of $PM_{2.5}$ estimation, the improvements in explained variances, the root-mean-square error (RMSE), normalized RMSE (NRMSE) and ratio of RMSE to standard deviation (RSR) are used.

2 INSTRUMENTS, DATA AND METHODS

2.1 $PM_{2.5}$ Measurements

NEA operates thirteen air quality monitoring stations in Singapore (NEA, 2011a), of which Pandan Reservoir station is nearest to the NUS atmospheric measurement supersite (~ 4 km; For supersite details, see Atwood et al., 2013; Chew et al., 2013; Salinas et al., 2013a). These stations are positioned strategically in industrial, urban and suburban areas, as well as along roadsides to monitor the ambient air quality. They are linked up via a telemetric monitoring and management system. The concentrations of major criteria pollutants (i.e. $PM_{2.5}$, PM_{10}, carbon monoxide, nitrogen oxide, carbon monoxide, and sulphur dioxide) are measured, and reported to the public daily. For this study, $PM_{2.5}$ measurements are applied as hourly averages.

At Pandan Reservoir, $PM_{2.5}$ concentrations are measured with the Thermo Scientific FH 62 C14 series continuous ambient particulate monitor. Air is first sampled via an aerosol inlet with cutoff diameter of 2.5 μm, which is heated above ambient temperature to remove condensation. Sampled particles are subsequently collected onto a filter tape between a Carbon-14 source and detector within the instrument. The instrument measures the concentration of sampled particles via the beta ray attenuation method (e.g., Hinds, 1999). The filter tape sample spot is advanced every hour, thus providing hourly $PM_{2.5}$ mass concentrations.

Due to the high RH in the region, aerosol hygroscopic growth influences the AOD-$PM_{2.5}$ relationship (Tsai et al., 2011; Chu et al., 2013). When particles containing hygroscopic components (e.g., sulfates and some organics) are exposed to high RH (> 70%), the scattering cross-section of particles undergoing substantial water absorption can increase by more than a factor of two (e.g., Hänel 1976). Even biomass burning particles, which are globally much less hygroscopic than anthropogenic emission counterparts, have a high hygroscopicity due to their high primary and/or secondary sulphur load – a result perhaps of the regions rich in volcanic soils (e.g., Reid et al., 2005; 2013). Based on the physics of highly soluble salts, the hygroscopic growth function is frequently written as

$$f(\mathrm{RH}) = \left(\frac{1 - \mathrm{RH}/100}{1 - \mathrm{RH_o}/100}\right)^{-g}, \quad (1)$$

where RH is in percentage, RH_o is referenced at 30 % and g is an empirical growth fitting parameter (Kasten, 1969). Values of g range from zero for insoluble particles to almost unity for highly soluble particles.

Due to the lack of aerosol hygroscopicity measurements from a dual nephelometer set-up (e.g., Hegg et al., 1996; Kotchenruther and Hobbs, 1998), which renders more constrained estimates, the hygroscopic growth function of a sulfate environment is assumed (i.e., g = 0.63; Hänel, 1976) and applied to the $PM_{2.5}$ measurements here. This assumption is supported by the observations of See et al. (2006) in reporting in situ measurements of aerosol microphysical properties at Singapore as consistent with that for a sulfate pollution environment (e.g., Waggoner and Weiss, 1980).

Hourly-averaged RH data are acquired from the National Climate Data Center (NCDC; http://www.ncdc.noa.gov), and used to compute f(RH). Although the annual average RH is 84.2%, Singapore experiences a diurnal variation from ~ 90% in the early morning to 60% in the mid-afternoon, even going below 50% at times (NEA, 2011b). During prolonged heavy rain, RH often approaches 100%. As substantial errors in the calculation of aerosol hygroscopic growth factor can be introduced when aerosol types are not properly identified, only data with RH $\leq$ 75% are used (e.g. Tsai et al., 2011; Chu et al., 2013) in this study.

2.2 AERONET and MPLNET

The Singapore AERONET site deploys a Cimel Electronique CE-318N sun photometer. The instrument collects direct solar measurements in eight spectral bands (with center wavelengths

from 0.340 μm to 1.640 μm) every 30 s within one-minute periods, which are then averaged as triplet measurements in order to derive AOD (Holben et al., 1998). Only cloud-screened (Smirnov et al., 2000) and quality-assured Level 2.0 AOD data are used in this study. The estimated accuracy of AERONET Cimels varies spectrally from ±0.01 to ±0.02 for AOD measurements with higher errors in the ultraviolet channels (Holben et al., 1998; Eck et al., 1999). Chew et al. (2011) found, however, that unscreened cirrus clouds significantly increase this relative uncertainty at Singapore, with potential cirrus artifact of 0.02 to 0.08 being common.

The collated Singapore MPLNET instrument (0.527 μm; Spinhirne, 1993; Spinhirne et al., 1995) is a compact and eye-safe mie lidar. The instrument is able to profile aerosol and cloud layers vertically by transmitting short laser pulses into the atmosphere and then measuring the backscattered signals. Instrument calibration includes corrections for detector dead-time, dark counts, afterpulsing and lidar overlap (Campbell et al., 2002). After subtracting the solar background signal, the raw profiles are then converted to MPLNET Level 1.0 Normalized Relative Backscatter (NRB) product, which is range- and energy-normalized. The uncertainties for the NRB product have been detailed in Welton and Campbell (2002).

MPLNET Level 1.0 NRB product are first screened for visible clouds (e.g., Clothiaux et al., 1998) and optically-thin cirrus clouds (e.g., Campbell et al., 2008; Chew et al., 2011; Campbell et al., 2015b), and subsequently averaged as 20-minute segments about AERONET Level 2.0 AOD observations. The former step helps filter potential error in collocated AERONET observations from unscreened cloudiness. Vertical profiles of aerosol particle backscatter and extinction coefficients are derived from these 20-minute averaged NRB data with the backward Fernald two-component solution to the lidar equation (Fernald, 1984; Welton et al., 2000). These profiles are considered quality-assured as MPLNET Level 2.0a aerosol product when they are acquired within

an optimal temperature range (23 ± 5 °C for the Singapore MPLNET instrument), have extinction-to-backscatter ratio error < 30%, and include > 80% of 20-minute averaged NRB data.

In this study, modified aerosol scale heights (H_m) are derived from the MPLNET Level 2.0a vertical profiles of extinction coefficient ($\beta(z)$ as a function of height z) such that approximately 63% of the total AOD exist below the point (e.g., Hayasaka et al., 2007; Turner et al., 2001):

$$\int_0^{H_m} \beta\,(z)\,dz \;=(1-\mathrm{e}^{-1})\mathrm{AOD} \;\cong\; 0.632\,\mathrm{AOD}\,. \qquad (2)$$

H_m is subsequently used to normalize AOD in order to estimate surface $PM_{2.5}$ concentrations. Although mean planetary boundary layer (PBL) extinctions can also be used to estimate surface $PM_{2.5}$ concentrations (e.g., Engel-Cox et al., 2006; Liu et al., 2011), the derivation of PBL heights over the region can be erroneous due to the frequent presence of low-level clouds causing deeper PBL height retrievals with the typical wavelet techniques (e.g., Brooks, 2003). At this point of time, MPLNET is processing all data, including that of Singapore, which will be collectively known as "Version 3" and includes an improved PBL height product (Welton, 2015; personal communication). The new PBL height retrieval algorithm uses image processing and fuzzy logic techniques to overcome the shortcomings of using wavelet techniques alone (Lewis et al., 2013).

Fig. 1 depicts seasonal H_m distributions over Singapore from October to December 2009 (OND 2009; Fig. 1a), January to March 2010 (JFM 2010; Fig. 1b), April to June (AMJ 2010; Fig. 1c), July to September (JAS 2010; Fig. 1d), October to December 2010 (OND 2010; Fig. 1e) and January to March 2011 (JFM; Fig. 1f), corresponding with the seasonal aerosol extinction coefficient profiles, lidar ratios and Ångström exponents reported in Chew et al. (2013). A bi-modal distribution with a mode below and above the top of strongly-capped/deep near-surface layer (SCD;

0 – 1.35 km; Chew et al., 2013) is found, consistent with the presence of vertical wind shear over Singapore, resulting in potential aerosol reservoirs aloft above the boundary layer (Atwood et al., 2013). The overall H_m distribution exhibits a mean of ~ 1.4 km, as summarized in Fig. 1g, with 42% of occurrence below and 58% of occurrence above the top of the SCD.

Yu et al. (2010) found CALIOP-derived seasonal H_m of ~ 1.4 – 1.9 km for the SEA region, generating seasonal H_m of ~ 1.7 – 2.1 km with the Goddard Chemistry Aerosol Radiation Transport (GOCART) model. While CALIPO-derived H_m are more consistent with the MPLNET-derived quantities, GOCART-derived quantities are consistently higher than ground- and satellite-based measurements, indicting a likely overestimation of aerosol transport within the free atmosphere.

2.3 MODIS Level 2 Aerosol Products

MODIS Collection 5.2 aerosol products (Level 2 MOD04 and MYDO4 for data collected from NASA Terra and Aqua satellite respectively) are available from the NASA Level 1 and Atmosphere Archive and Distribution System (LAADS). Alternatively, the data can be generated with the International MODIS/AIRS Processing Package (IMAPP; http://cimss.ssec.wisc.edu/imapp/) for ground stations capable of receiving direct broadcast from the Terra and Aqua satellites, which can be advantageous for monitoring air pollution in near real time. For this study, the AOD measurements at 0.55 μm (Optical_Depth_Land_And_Ocean variable of MOD04 and MYDO4 aerosol product) with a nominal spatial resolution of 10 by 10 km (Remer et al., 2005) are used. The actual ground footprint for these satellite AOD data ranges from 10 by 10 km at nadir to roughly 40 by 20 km at the edge of the satellite swath.

2.4 NAAPS aerosol transport model and FLAMBE smoke flux model

The NAAPS model is a modified form of a hemispheric model of sulfate aerosols developed by Christensen (1997), with dust, biomass burning smoke and sea salt as described by Westphal et al., 2009; Reid et al., 2009; and Witek et al., 2007, respectively. For this study period, NAAPS is driven by meteorological fields from the Navy Operational Global Atmospheric Prediction System (NOGAPS; e.g., Hogan and Rosmond, 1991; Hogan and Brody, 1993). Smoke, dust and sulfate AOD, as well as aerosol mass concentrations, are determined at a 1° × 1° grid for this study in 6-h intervals and twenty-four vertical levels up to 100 mb. The Naval Research Laboratory (NRL) Atmospheric Variational Data Assimilation System – Aerosol Optical Depth (NAVDAS-AOD; Zhang et al, 2008) is used to improve NAAPS model simulations by assimilating MODIS AOD data over sea and land within the modeled fields (Hyer et al., 2011; Shi et al., 2011).

The Fire Locating and Monitoring of Burning Emissions (FLAMBE) smoke flux model is applied to estimate biomass burning emissions within NAAPS (Reid et al., 2004; 2009). MODIS active fire detections are used to determine the locations and timings of fires (Giglio et al., 2003), which are subsequently mapped onto the Global Land Cover Classification (GLCC Version 2.0; Loveland and Belward, 1997) 1-km land cover map to estimate burning fuels. The resultant fire intensive properties (i.e., fuel loading, fuel consumption, emission partitioning according to various aerosol species) are then calculated based on the fuel models of Reid et al. (2005).

Hyer and Chew (2010) have previously used NAAPS analyses to examine an extreme MC biomass burning smoke episode from September to October 2006. In that study, NAAPS was able to capture the timing of smoke events, but severely underestimated their magnitude. Campbell et al. (2015) recently conclude a similar result, having paired FLAMBE with WRF-Chem and examining 3-5 day smoke transport across Borneo Island. These studies indicate that FLAMBE is not fully resolving the variability in smoke emissions. Though, based on MODIS overpasses alone, this is to be expected given only four possible views of a given scene per day and only a coarse

mapping of available fuel sources. Based on a regression analysis between the measured daily PM_{10} concentrations and NAAPS surface concentrations at 54 air quality monitoring stations in Singapore and Malaysia, we estimate that FLAMBE is underestimating regional smoke emissions by a factor of between 2.5 to 10, and a overall correction factor of 3.5 is approximated. This correction factor is similar to other regional studies conducted at the mesoscale (e.g., Wang et al., 2013).

3 RESULTS AND DISCUSSION

3.1 Correlation between MPLNET-derived extinction coefficients and hygroscopic-corrected $PM_{2.5}$ measurements

After constraining our data sample for cases of RH $\leq$ 75%, there are a total of 855 AERONET Level 2.0 data coincident with cloud-free MPLNET-derived vertical profiles of aerosol particle extinction available for analysis. In order to match the temporal resolution of the $PM_{2.5}$ measurements, available AERONET and MPLNET data are also hourly averaged (N = 205).

MPLNET-derived extinction coefficients at 100-m intervals from 0 to 2.4 km are compared with hygroscopic-corrected surface $PM_{2.5}$ concentrations, with the resultant coefficients of determination (R^2) shown in Table 1.It should be noted that overlap corrections can be significant for heights lower than 200 m (Campbell et al., 2002; Toth et al., 2014). Correlations between the two are moderate (R^2 ~ 0.35 – 0.54) from 0 – 1.2 km, which includes the SCD. Above 1.3 km, correlation between the two is substantially reduced (R^2 ~ 0.03 – 0.29; not shown). Higher correlation within the SCD may be the result of strong vertical mixing produced by updrafts due to high surface temperatures over Singapore (e.g., Li et al., 2013). As such, a mean extinction coefficient within the mixed layer is likely more suitable than a series of contiguous near-surface

extinction coefficients for comparison with hourly-average $PM_{2.5}$ measurements, taking into account possible vertical mixing within an hourly time frame.

3.2 Correlation between AERONET AOD and hygroscopic-corrected $PM_{2.5}$ measurements

H_m derived from MPLNET Level 2.0a data are used to scale AERONET, MODIS and NAAPS AOD to approximate a near surface extinction coefficient for comparison with ground-level $PM_{2.5}$ measurements, similar to the methods described in Tsai et al. (2011) and Chu et al. (2013). Substantial variability in aerosol vertical distributions exists over Singapore (Chew et al., 2013), due primarily to vertical wind shear and the potential for aerosol reservoirs aloft above the boundary layer (e.g., Atwood et al., 2013). Therefore, scaling the columnar AOD by the modified aerosol scale height is a simple method that takes into account the possible air mass exchange between the boundary layer and free troposphere.

Fig. 2 features correlation between AERONET AOD and hygroscopic-corrected $PM_{2.5}$ concentration as aerosol scale height corrections are applied. Correlation is high ($R^2 \sim 0.47 – 0.58$), with an increase of 11% in explained variances (from the difference in R^2 values) when aerosol scale height corrections are applied. Scatter about the regression line is also noticeably reduced.

In order to further evaluate the models of $PM_{2.5}$ estimation by AOD and AOD/H_m , we calculate RMSE, NRMSE and RSR for the AERONET data in Table 2, together with MODIS and NAAPS data for comparison (e.g., Chu et al., 2013). RMSE indicates the difference between the fitted and observed data, whereas NRMSE also considers the range, i.e. the maximum and minimum, of the observed data. RSR further compares the uncertainty of $PM_{2.5}$ estimated from AOD and AOD/H_m, to the observations. RMSE (10.32 – 11.61 μg m^{-3}) is comparable with NAAPS data, but NRMSE (0.10 – 0.11) is the lowest among all the data. The hygroscopic-corrected $PM_{2.5}$

as estimated by AERONET data has the lowest RSR (0.65 – 0.73) among all the data, as well as an improvement of 8 % in RSR when using scaled AERONET AOD.

3.3 Correlation between MODIS AOD and hygroscopic-corrected $PM_{2.5}$ measurements

In order to spatially correlate ground measurements (i.e. MPLNET-derived H_m and $PM_{2.5}$ concentrations) with satellite-based MODIS AOD, they are paired up with a satellite observation by choosing image pixels that are spatially and temporally close. First, only ground measurements within an hour of the satellite observations are considered for correlation. Second, all satellite observations within 0.50° (~ 40 – 50 km) of the measurement supersite are spatially averaged, due to the constant cloud coverage over Singapore preventing otherwise routine data acquisition. Such separation requirements are consistent with the lagged correlation analysis conducted for surface measurements against sky-based and space-based measurements by Anderson et al. (2003).

Although 220 MODIS AOD observations are available from September 2009 to March 2011, only 38 observations are available for comparison with ground measurements due to separation requirements. Fig. 3a illustrates the relatively tenuous relationship between AERONET and MODIS AOD (R^2 = 0.54). Despite small differences in sampling methodology, Hyer et al. (2011) found varying slopes from 0.76 (Mukdahan; 17° N, 105° E) to 1.52 (Bac Lieu; 9° N and 106° E) when comparing between AERONET and MODIS AOD in SEA due to the complex aerosol and land surface environment.

Fig. 3b and c depict correlation between MODIS AOD and hygroscopic-corrected $PM_{2.5}$ concentration as aerosol scale height corrections are applied. The correlation for MODIS is weaker when compared with AERONET, although improvements (from R^2 of 0.35 to 0.45) are noted with an increase of 10% in explained variances (from the difference in R^2 values) when aerosol scale height corrections are applied. The primary reason for the lesser correlation is attributed to constant

cloud cover and contamination over the region, resulting in less quality-assured MODIS AOD retrievals available near Singapore. Spatial averaging of MODIS AOD to compensate for cloud cover is also likely to reduce representativeness.

RMSE, NRMSE and RSR are also calculated for MODIS data in Table 2. Although RMSE (7.90 – 8.55 μg m^{-3}) is the lowest among all the data, this result is likely an artifact due to the small sample size. NRMSE (0.22 – 0.23) for MODIS data is the largest among all the data, and is indicative that RMSE is large compared to the observed data range. When using MODIS AOD/H_m instead of AOD to estimate hygroscopic-corrected $PM_{2.5}$, there is an improvement of 6 % in RSR (from 0.82 to 0.76).

3.4 Correlation between NAAPS AOD, surface concentrations and hygroscopic-corrected $PM_{2.5}$ measurements

As satellite observations over Singapore are limited by relatively frequent cloud cover, NAAPS AOD can be considered a first-order proxy for MODIS AOD, and has in fact been shown to correlate well with MODIS in Southeast Asia in the 00 hr model analysis state through verification with AERONET (Campbell et al., 2013). In order to spatially correlate NAAPS AOD and surface concentration with ground measurements (i.e. MPLNET-derived H_m and $PM_{2.5}$ concentrations), only output from the nearest NAAPS model grid are used and interpolated with regards to time. There exists an extreme outlier when comparing the AERONET and NAAPS AOD (not shown), which is subsequently removed.

Fig. 4a features correlation between NAAPS surface concentration and $PM_{2.5}$ concentration. Despite AOD data assimilation, NAAPS underestimates surface level concentrations over Singapore, as previously observed by Hyer and Chew (2010) for PM_{10} concentrations. NAAPS representation of near surface processes is limited by the coarse model

spatial resolution and rapid vertical mixing scheme among the lowest model layers, thus aerosol vertical distributions and surface concentrations are not realistically simulated.

In contrast, AOD is a columnar optical quantity, which is not affected by aforementioned model limitations. Fig. 4b and c reflect reasonable correlation between NAAPS AOD and hygroscopic-corrected $PM_{2.5}$ concentration ($R^2 \sim 0.22 – 0.27$) with and without aerosol scale height corrections, respectively. However, any improvement in correlation from applying the aerosol scale height corrections is considered marginal, as there is only 5% increase in explained variance (see difference in R^2 values).

RMSE, NRMSE and RSR are calculated for NAAPS data in Table 2. RMSE (12.82 – 13.24 $\mu g\ m^{-3}$) is comparable to AERONET data. NRMSE (0.16) is similar to AERONET data, and lower than MODIS data due to the large sample size. There is also slight improvement of 2 % in RSR (from 0.88 to 0.86) when using scaled NAAPS AOD. These results are possibly due to model-related issues as discussed in Hyer and Chew (2010), especially the deficiencies in the emission database. A recent field experiment in Southeast Asia investigated MPLNET aerosol extinction profiles versus those derived from the Weather Research and Forecasting model coupled with Chemistry (WRF-Chem) using FLAMBE as the emissions (Wang et al., 2013; Campbell et al., 2015a). Despite the higher model resolution allowed in WRF-Chem compared with NAAPS, model-derived aerosol extinctions are still mostly underestimated, as described above. Similarly, regional cloud cover prevents effective MODIS data acquisition and assimilation for NAAPS. Cloud bias in MODIS data can also be so severe in the region that it decreases model efficacy when unscreened observations are assimilated (Reid et al., 2009; Hyer et al., 2011).

4 CONCLUSIONS

In the study, the relationships between Aerosol Robotic Network (AERONET), Moderate Resolution Imaging Spectroradiometer (MODIS), Navy Aerosol Analysis and Prediction System (NAAPS) aerosol optical depth (AOD) and particulate matter with aerodynamic equivalent diameter of less than 2.5 μm ($PM_{2.5}$) concentrations over Singapore for potential air quality applications are examined using coincident AERONET Level 2.0 and MPLNET Level 2.0a datasets from 24 September 2009 to 31 March 2011. The modified aerosol scale height (H_m), which represents the vertical extent of aerosols (Hayasaka et al., 2007), are derived to scale columnar AOD to approximate near surface extinction for comparison with surface $PM_{2.5}$ measurements. This approach is similar to the methods described in Chu et al. (2013) and Tsai et al. (2011), which normalized columnar MODIS AOD with a combined planetary boundary layer height (PBL) and a scale height of exponential decay of aerosol extinction above the PBL. The conclusions are as follow:

1. The H_m distribution over Singapore is observed to be bimodal with a mode below and another mode above the top of strongly-capped/deep near-surface layer (SCD; 0 – 1.35 km; Chew et al., 2013). The mean H_m of 1.4 km is derived, which is comparable to CALIOP-derived seasonal H_m of ~ 1.4 km – 1.9 km over the SEA region (Yu et al., 2010).
2. MPLNET-derived near surface extinctions (0 – 1.3 km) are well correlated with surface $PM_{2.5}$ concentrations (R^2 ~ 0.29 – 0.54) within the SCD layer, which may be due to strong vertical mixing caused by high surface temperature (Li et al., 2013). Above 1.3 km, the correlations are substantially reduced (R^2 ~ 0.03 – 0.21).
3. The AERONET and MODIS AOD-$PM_{2.5}$ correlations are improved (i.e. from R^2 of 0.47 to 0.58, and from R^2 of 0.35 to 0.45, respectively) when applying aerosol scale

height corrections, with an increase of 11% and 10% of explained variance respectively. There are also improvements of 8 % and 6 % when considering the ratio of root mean square error to standard deviation (RSR) for AERONET and MODIS AOD respectively.

4. The NAAPS AOD-$PM_{2.5}$ correlation changes marginally (i.e. from R^2 of 0.22 to 0.27) when applying aerosol scale height corrections, with a slight increase of 5% in explained variance. There is also a slight improvement of 2 % when considering RSR for NAAPS AOD. NAAPS surface concentration is also not well correlated with $PM_{2.5}$ concentrations. The weaker correlations are possibly due to the deficiencies in the FLAMBE database for the region.

With the imminent launch of earth observation satellites at an near-equatorial orbit, such as Singapore's Temasek Low Earth Orbit Satellite (TeLEOS-1) and Kent Ridge satellite (KR-1), as well as geostationary satellites, such as Himawari-8/9 (http://www.data.jma.go.jp/mscweb/en/himawari89/index.html), more frequent passes over the region will provide timely monitoring of air pollution and observations of extreme biomass burning smoke. This will increase regional coverage, compared with sun-synchronous instruments like MODIS, and thus provide additional opportunity to alleviate data-denial conditions induced by endemic cloud cover. Further, greater satellite coverage, and corresponding aerosol observations, will allow better estimations of surface aerosol concentration, providing more data for civil authorities and more assimilable data for model systems.

ACKNOWLEDGEMENTS:

AERONET and MPLNET are supported with funding from the NASA Earth Observing System and Radiation Sciences Programs. The AERONET and MPLNET instruments are deployed to Singapore as part of the Seven Southeast Asian Studies (7 SEAS) field campaign, as sponsored by the Office of Naval Research (ONR), ONR Global and NASA. The authors would like to thank Singapore's National Environment Agency (NEA) for collecting and archiving the surface air quality data.

REFERENCES:

Anderson, T.L., Charlson, R.J., Winker, D.M., Ogren, J.A., Holmén, K. (2003). Mesoscale Variations of Tropospheric Aerosols. J. Atmos. Sci. 60: 119–136.

Atwood, S.A., Reid, J.S., Kreidenweis, S., Yu, L.E., Salinas, S.V., Chew, B.N., Balasubramanian, R. (2013). Analysis of source regions for smoke events in Singapore for the 2009 El Nino burning season. Atmos. Environ. 78: 219–230.

Bilal, M., Nichol, J.E., Bleiweiss, M.P., Dubois, D. (2013). A Simplified high resolution MODIS Aerosol Retrieval Algorithm (SARA) for use over mixed surfaces. Remote Sens. Environ. 136: 135-145.

Brooks, I.M. (2003). Finding Boundary Layer Top: Application of a Wavelet Covariance Transform to Lidar Backscatter Profiles. J. Atmos. Ocean. Technol. 20: 1092–1105.

Campbell, J.R., Hlavka, D.L., Welton, E.J., Flynn, C.J., Turner, D.D., Spinhirne, J.D., Scott, V.S., Hwang, I.H. (2002). Full-time, eye-safe cloud and aerosol lidar observation at atmospheric radiation measurement program sites: instrument and data processing. J. Atmos. Oceanic Technol. 19: 431–442.

Campbell, J.R., Sassen K., Welton, E.J. (2008). Elevated cloud and aerosol layer retrievals from micropulse lidar signal profiles. J. Atmos. Oceanic Technol. 25: 685-700.

Campbell, J.R., Reid, J.S., Westphal, D.L., Zhang, J., Tackett, J.L., Chew, B.N., Welton, E.J., Shimizu, A., Sugimoto, N., Aoki K., Winker, D.M. (2013). Characterizing the vertical profile of aerosol particle extinction and linear depolarization over Southeast Asia and the Maritime Continent: the 2007-2009 view from CALIOP. Atmos. Res. 122: 520 - 543.

Campbell, J.R., Ge., C., Wang, J., Welton, E.J., Lolli, S., Bucholtz, A., Hyer, E.J., Reid, E.A., Chew, B.N., Liew, S.C., Salinas, S.V., Mahamod, M., Mohamad, M., Holben, B.N. (2015a). Applying advanced ground-based remote sensing in the Southeast Asian Maritime Continent to

447 characterize regional proficiencies in smoke transport modeling. J. Appl. Meteorol. Clim.
448 (Accepted).
449 Campbell, J.R., Vaughan, M.A., Oo, M., Holz, R.E., Lewis, J.R., Welton, E.J. (2015b).
450 Distinguishing cirrus cloud presence in autonomous lidar measurements. Atmos. Meas. Tech.,
451 8: 435-449.
452 Chew, B.N., Campbell, J.R., Reid, J.S., Giles, D.M., Welton, E.J., Salinas, S.V., Liew, S.C. (2011).
453 Tropical cirrus cloud contamination in sun photometer data. Atmos. Environ. 45: 6724-6731.
454 Chew, B.N., Campbell, J.R., Salinas, S. V., Chang, C.W., Reid, J.S., Welton, E.J., Holben, B.N.,
455 Liew, S.C. (2013). Aerosol particle vertical distributions and optical properties over Singapore.
456 Atmos. Environ. 79: 599–613.
457 Christensen, J.H. (1997). The Danish eulerian hemispheric model – a three-dimensional air
458 pollution model used for the Arctic. Atmos. Environ. 31: 4169–4191.
459 Chu, D.A., Kaufman, Y.J., Zibordi, G., Chern, J.D., Mao, J., Li, C., Holben, B.N. (2003). Global
460 monitoring of air pollution over land from the Earth Observing System-Terra Moderate
461 Resolution Imaging Spectroradiometer (MODIS). J. Geophys. Res. 108: 4661.
462 Chu, D.A., Tsai, T.-C., Chen, J.-P., Chang, S.-C., Jeng, Y.-J., Chiang, W.-L., Lin, N.-H. (2013).
463 Interpreting aerosol lidar profiles to better estimate surface $PM_{2.5}$ for columnar AOD
464 measurements. Atmos. Environ. 79: 172–187.
465 Diner, D., Beckert, J., Bothwell, G., Rodriguez, J. (2002). Performance of the MISR instrument
466 during its first 20 months in earth orbit. IEEE Trans. Geosci. Remote Sens. 40: 1449−1466.
467 Eck, T.F., Holben, B.N., Reid, J.S., Dubovik, O., Smirnov, A., O'Neill, N.T., Slutsker, I., Kinne,
468 S. (1999). Wavelength dependence of the optical depth of biomass burning, urban, and desert
469 dust aerosols. J. Geophys. Res. 104: 31333.
470 Engel-Cox, J.A., Holloman, C.H., Coutant, B.W., Hoff, R.M. (2004). Qualitative and quantitative

evaluation of MODIS satellite sensor data for regional and urban scale air quality. Atmos. Environ. 38: 2495–2509.

Engel-Cox, J.A., Hoff, R.M., Rogers, R., Dimmick, F., Rush, A.C., Szykman, J.J., Al-Saadi, J., Chu, D.A., Zell, E.R. (2006). Integrating lidar and satellite optical depth with ambient monitoring for 3-dimensional particulate characterization. Atmos. Environ. 40: 8056–8067.

Field, R.D., van der Werf, G.R., Shen, S.S.P. (2009). Human amplification of drought-induced biomass burning in Indonesia since 1960. Nat. Geosciences 2: 185–188.

Giglio, L., Descloitres, J., Justice, C.O., Kaufman, Y.J. (2003). An Enhanced Contextual Fire Detection Algorithm for MODIS. Remote Sens. Environ. 87: 273–282.

Gupta, P., Christopher, S.A. (2009a). Particulate matter air quality assessment using integrated surface, satellite, and meteorological products: Multiple regression approach. J. Geophys. Res. 114: D14205.

Gupta, P., Christopher, S.A. (2009b). Particulate matter air quality assessment using integrated surface, satellite, and meteorological products: 2. A neural network approach. J. Geophys. Res. 114: D20205.

Gupta, P., Christopher, S.A., Wang, J., Gehrig, R., Lee, Y., Kumar, N. (2006). Satellite remote sensing of particulate matter and air quality assessment over global cities. Atmos. Environ. 40: 5880–5892.

Hänel, G. (1976). The properties of atmospheric aerosol particles as functions of relative humidity at thermodynamic equilibrium with surrounding moist air. Adv. Geophys. 19: 73–188.

Hayasaka, T., Meguro, Y., Sasano, Y., Takamura, T. (1998). Stratification and Size Distribution of Aerosols Retrieved from Simultaneous Measurements with Lidar, a SunPhotometer, and an Aureolemeter. Appl. Opt. 37: 961–970.

Hayasaka, T., Satake, S., Shimizu, A., Sugimoto, N., Matsui, I., Aoki, K., Muraji, Y. (2007). Vertical distribution and optical properties of aerosols observed over Japan during the Atmospheric Brown Clouds–East Asia Regional Experiment 2005. J. Geophys. Res. 112: D22S35.

Hegg, D.A., Covert, D.S., Rood, M.J., Hobbs, P. V. (1996). Measurements of aerosol optical properties in marine air. J. Geophys. Res. 101: 12893.

Hinds, W.C. (1999). Aerosol Technology: Properties, Behavior, and Measurement of Airborne Particles. Wiley-Interscience.

Hidy, G.M., Brook, J.R., Chow, J.C., Green, M., Husar, R.B., Lee, C., Scheffe, R.D., Swanson, A., Watson, J.G. (2009). Remote Sensing of Particulate Pollution from Space: Have We Reached the Promised Land? J. Air Waste Manage. Assoc. 59: 1130–1139.

Hoff, R.M., Christopher, S.A. (2009). Remote sensing of particulate pollution from space: have we reached the promised land? J. Air Waste Manag. Assoc. 59: 645–75; discussion 642–644.

Hogan, T.F., Brody, L.R. (1993). Sensitivity studies of the Navy's global forecast model parameterizations and evaluation of improvements to NOGAPS. Mon. Weather Rev. 121: 2373–2395.

Hogan, T.F., Rosmond, T.E. (1991). The description of the Navy operational global atmospheric prediction system's spectral forecast model. Mon. Weather Rev. 119: 1786–1815.

Holben, B.N., Eck, T.F., Slutsker, I., Tanré, D., Buis, J.P., Setzer, A., Vermote, E., Reagan, J.A., Kaufman, Y.J., Nakajima, T., Lavenu, F., Jankowiak, I., Smirnov, A. (1998). AERONET—A Federated Instrument Network and Data Archive for Aerosol Characterization. Remote Sens. Environ. 66: 1–16.

Hyer, E.J., Chew, B.N. (2010). Aerosol transport model evaluation of an extreme smoke episode in Southeast Asia. Atmos. Environ. 44: 1422–1427.

519 Hyer, E.J., Reid, J.S., Zhang, J. (2011). An over-land aerosol optical depth data set for data
520 assimilation by filtering, correction, and aggregation of MODIS Collection 5 optical depth
521 retrievals. Atmos. Meas. Tech. 4: 379–408.
522 Kasten F. (1969). Visibility in the phase of pre-condensation. Tellus 21: 631–635.
523 Kim, P.S., Jacob, D.J., Mickley, L., Koplitz, S., Marlier, M.E., DeFries, R., Myers, S.S., Chew,
524 B.N., Mao, Y.H. (2014). Sensitivity of population smoke exposure to fire locations in Equatorial
525 Asia. Atmos. Environ. 102: 11–17.
526 Kotchenruther, R.A., Hobbs, P. V. (1998). Humidification factors of aerosols from biomass
527 burning in Brazil. J. Geophys. Res. 103: 32081.
528 Kumar, N., Chu, A., Foster, A. (2007). An empirical relationship between $PM_{2.5}$ and aerosol optical
529 depth in Delhi Metropolitan. Atmos. Environ. 41: 4492–4503.
530 Lewis, J.R., Welton, E.J., Molod, A.M., Joseph, E. (2013). Improved boundary layer depth
531 retrievals from MPLNET. J. Geophys. Res. Atmos. 118: 9870-9879.
532 Li, C., Lau, A.K.-H., Mao, J., Chu, D.A. (2005). Retrieval, validation, and application of the 1-km
533 aerosol optical depth from MODIS measurements over Hong Kong. IEEE Trans. Geosci.
534 Remote Sens. 43: 2650–2658.
535 Li, X.-X., Koh, T.-Y., Entekhabi, D., Roth, M., Panda, J., Norford, L.K. (2013). A multi-resolution
536 ensemble study of a tropical urban environment and its interactions with the background
537 regional atmosphere. J. Geophys. Res. 118: 9804–9818.
538 Liu, Y., Park, R.J., Jacob, D.J., Li, Q., Kilaru, V., Sarnat, J.A. (2004). Mapping annual mean
539 ground-level $PM_{2.5}$ concentrations using Multiangle Imaging Spectroradiometer aerosol optical
540 thickness over the contiguous United States. J. Geophys. Res. 109: D22206.
541 Liu, Y., Sarnat, J.A., Kilaru, V., Jacob, D.J., Koutrakis, P. (2005). Estimating Ground-Level $PM_{2.5}$
542 in the Eastern United States Using Satellite Remote Sensing. Environ. Sci. Technol. 39: 3269–

3278.

Liu, Y., Wang, Z., Wang, J., Ferrare, R.A., Newsom, R.K., Welton, E.J. (2011). The effect of aerosol vertical profiles on satellite-estimated surface eparticle sulfate concentrations. Remote Sens. Environ. 115: 508 – 513.

Loveland, T.R., Belward, A.S. (1997). The IGBP-DIS global 1km land cover data set, DISCover: First results. Int. J. Remote Sens. 18: 3289–3295.

National Environment Agency (2011a). Environmental Protection Department Annual Report. National Environment Agency, Singapore.

National Environment Agency (2011b). Weather Statistics. Available at http://app2.nea.gov.sg/weather-climate/climate-information/weather-statistics.

Reid, J.S., Prins, E.M., Westphal, D.L., Schmidt, C.C., Richardson, K.A., Christopher, S.A., Eck, T.F., Reid, E.A., Curtis, C.A., Hoffman, J.P. (2004). Real-time monitoring of South American smoke particle emissions and transport using a coupled remote sensing/box-model approach. Geophys. Res. Lett. 31: L06107.

Reid, J.S., Eck, T.F., Christopher, S.A., Koppmann, R., Dubovik, O., Eleuterio, D.P., Holben, B.N., Reid, E.A., Zhang, J. (2005). A review of biomass burning emissions part III: intensive optical properties of biomass burning particles. Atmos. Chem. Phys. 5: 827–849.

Reid, J.S., Hyer, E.J., Prins, E.M., Westphal, D.L., Zhang, J., Wang, J., Christopher, S.A., Curtis, C.A., Schmidt, C.C., Eleuterio, D.P., Richardson, K.A., Hoffman, J.P. (2009). Global monitoring and forecasting of biomass-burning smoke: description of and lessons from the fire locating and modeling of burning emissions (FLAMBE) program. IEEE J. Selected Topics Appl. Earth Observ. Rem. Sens. 2: 144-162.

Reid, J.S., Hyer, E.J., Johnson, R.S., Holben, B.N., Yokelson, R.J., Zhang, J., Campbell, J.R., Christopher, S.A., Di Girolamo, L., Giglio, L., Holz, R.E., Kearney, C., Miettinen, J., Reid,

E.A., Turk, F.J., Wang, J., Xian, P., Zhao, G., Balasubramanian, R., Chew, B.N., Janjai, S., Lagrosas, N., Lestari, P., Lin, N.-H., Mahmud, M., Nguyen, A.X., Norris, B., Oanh, N.T.K., Oo, M., Salinas, S. V., Welton, E.J., Liew, S.C. (2013). Observing and understanding the Southeast Asian aerosol system by remote sensing: An initial review and analysis for the Seven Southeast Asian Studies (7SEAS) program. Atmos. Res. 122: 403–468.

Remer, L.A., Kaufman, Y.J., Tanré, D., Mattoo, S., Chu, D. a., Martins, J. V., Li, R.-R., Ichoku, C., Levy, R.C., Kleidman, R.G., Eck, T.F., Vermote, E., Holben, B.N. (2005). The MODIS Aerosol Algorithm, Products, and Validation. J. Atmos. Sci. 62: 947–973.

Salinas, S. V., Chew, B.N., Liew, S.C. (2009). Retrievals of aerosol optical depth and Angström exponent from ground-based Sun-photometer data of Singapore. Appl. Opt. 48: 1473–1484.

Salinas, S. V., Chew, B.N., Miettinen, J., Campbell, J.R., Welton, E.J., Reid, J.S., Yu, L.E., Liew, S.C. (2013a). Physical and optical characteristics of the October 2010 haze event over Singapore: A photometric and lidar analysis. Atmos. Res. 122: 555–570.

Salinas, S.V., Chew, B.N., Mohamad, M., Mahmud, M., Liew, S.C. (2013b). First measurements of aerosol optical depth and Ångström exponent number from AERONET's Kuching site. Atmos. Environ. 78: 231–241.

Schaap, M., Apituley, A., Timmermans, R.M.A., Koelemeijer, R.B.A., de Leeuw, G. (2008). Exploring the relation between aerosol optical depth and $PM_{2.5}$ at Cabauw, the Netherlands. Atmos. Chem. Phys. Discuss. 8: 17939–17986.

See, S.W., Balasubramanian, R., Wang, W. (2006). A study of the physical, chemical, and optical properties of ambient aerosol particles in Southeast Asia during hazy and nonhazy days. J. Geophys. Res. 111: D10S08.

See, S.W., Balasubramanian, R., Rianawati, E., Karthikeyan, S., Streets, D.G. (2007). Characterization and source apportionment of particulate matter < or = 2.5 micrometer in

591 Sumatra, Indonesia, during a recent peat fire episode. Environ. Sci. Technol. 41: 3488–3494.
592 Shi, Y., Zhang, J., Reid, J.S., Holben, B.N., Hyer, E.J., Curtis, C. (2011). An analysis of the
593 collection 5 MODIS over-ocean aerosol optical depth product for its implication in aerosol
594 assimilation. Atmos. Chem. Phys. 11: 557–565.
595 Smirnov, A., Holben, B.N., Eck, T.F., Dubovik, O., Slutsker, I. (2000). Cloud-Screening and
596 Quality Control Algorithms for the AERONET Database. Remote Sens. Environ. 73: 337–349.
597 Spinhirne, J.D. (1993). Micro pulse lidar. IEEE Trans. Geosci. Remote Sens. 31: 48–55.
598 Spinhirne, J.D., Rall, J.A.R., Scott, V.S. (1995). Compact eye safe lidar systems. Rev. Laser Eng.
599 23: 112–118.
600 Tsai, T.-C., Jeng, Y.-J., Chu, D.A., Chen, J.-P., Chang, S.-C. (2011). Analysis of the relationship
601 between MODIS aerosol optical depth and particulate matter from 2006 to 2008. Atmos.
602 Environ. 45: 4777–4788.
603 Toth, T.D., Zhang, J., Campbell, J.R., Hyer, E.J., Reid, J.S., Shi, Y. ,Westphal, D.L. (2014). Impact
604 of data quality and surface-to-column representativeness on the $PM_{2.5}$/satellite AOD
605 relationship for the Continental United States. Atmos. Chem. Phys. 14: 6049-6062.
606 Turner, D.D., Ferrare, R. A., Brasseur, L. A. (2001). Average aerosol extinction and water vapor
607 profiles over the Southern Great Plains. Geophys. Res. Lett. 28: 4441–4444.
608 Waggoner, A.P., Weiss, R.E. (1980). Comparison of fine particle mass concentration and light
609 scattering extinction in ambient aerosol. Atmos. Environ. 14: 623–626.
610 Wang, J., Christopher, S.A. (2003). Intercomparison between satellite-derived aerosol optical
611 thickness and PM 2.5 mass: Implications for air quality studies. Geophys. Res. Lett. 30: 2095.
612 Wang, J., Ge, C., Yang, Z., Hyer, E.J., Reid, J.S., Chew, B.N., Mahmud, M., Zhang, Y., Zhang,
613 M. (2013). Mesoscale modeling of smoke transport over the Southeast Asian Maritime
614 Continent: Interplay of sea breeze, trade wind, typhoon, and topography. Atmos. Res. 122:

615 486–503.
616 Welton, E.J., Campbell, J.R. (2002). Micropulse Lidar Signals: Uncertainty Analysis. J. Atmos.
617 Ocean. Technol. 19: 2089–2094.
618 Welton, E.J., Campbell, J.R., Spinhirne, J.D., Scott, V.S. (2001). Global monitoring of clouds and
619 aerosols using a network of micro-pulse lidar systems. Proc. Int. Soc. Opt. Eng. 4153: 151–
620 158.
621 Westphal, D.L., Curtis, C.A., Liu, M., and Walker, A.L. (2009). Operational aerosol and dust storm
622 forecasting. In WMO/GEO Expert Meeting on an International Sand and Dust Storm Warning
623 System. IOP Conference Series Earth and Environmental Science, Vol 7, Perez, J. C., and
624 Baldasano, J. M. (Eds.).
625 Witek, M., Flatau, P.J., Quinn, P.K., and Westphal, D.L. (2007). Global seasalt modeling: Results
626 and validation against multicampaign shipboard measurements. J. Geophys. Res. 112: D08215.
627 Wong, M.S., Nichol, J., Lee, K.H., Lee, B.Y. (2011). Monitoring 2.5 μm particulate matter within
628 urbanized regions using satellite-derived aerosol optical thickness, a study in Hong Kong. Int.
629 J. Remote Sens. 32: 8449–8462.
630 Yu, H., Chin, M., Winker, D.M., Omar, A.H., Liu, Z., Kittaka, C., Diehl, T. (2010). Global view
631 of aerosol vertical distributions from CALIPSO lidar measurements and GOCART simulations:
632 Regional and seasonal variations. J. Geophys. Res. 115: D00H30.
633 Zhang, J., Reid, J.S., Westphal, D.L., Baker, N.L., Hyer, E.J. (2008). A system for operational
634 aerosol optical depth data assimilation over global oceans. J. Geophys. Res. 113: D10208.
635

636 # FIGURE CAPTIONS:

637 **Figure 1.** Seasonal modified aerosol scale height distributions detected by MPLNET instrument
638 at 0.527 μm over Singapore for (a) OND 2009, (b) JFM, (c) AMJ, (d) JAS, (e) OND 2010 and (f)
639 JFM 2011. (g) Overall modified aerosol scale height distribution. Bin sizes are 0.2 km. Blue
640 dashed line marks top of the SCD layer (0 – 1.35 km).

641

642 **Figure 2.** Correlation between (a) AERONET AOD and hygroscopic-corrected $PM_{2.5}$
643 concentration, and (b) AOD/H_m and hygroscopic-corrected $PM_{2.5}$ concentration. The text within
644 each panel describes the coefficient of determination (R^2), significance level of correlation (P, not
645 significant when P greater than 0.05), number of comparison pairs (N), root-mean-square error
646 (RMSE), and mean ± standard deviation of measured quantities.

647

648 **Figure 3.** (a) Validation between AERONET and MODIS AOD over Singapore. Correlation
649 between (b) MODIS AOD and hygroscopic-corrected $PM_{2.5}$ concentration, and (c) AOD/H_m and
650 hygroscopic-corrected $PM_{2.5}$ concentration. Text description within (b) and (c) is the same as for
651 Figure 2.

652

653 **Figure 4.** Correlation between (a) NAAPS surface concentration and $PM_{2.5}$ concentration, (b)
654 NAAPS AOD and hygroscopic-corrected $PM_{2.5}$ concentration, and (c) AOD/H_m and hygroscopic-
655 corrected $PM_{2.5}$ concentration. Text description within panels is the same as for Figure 2.

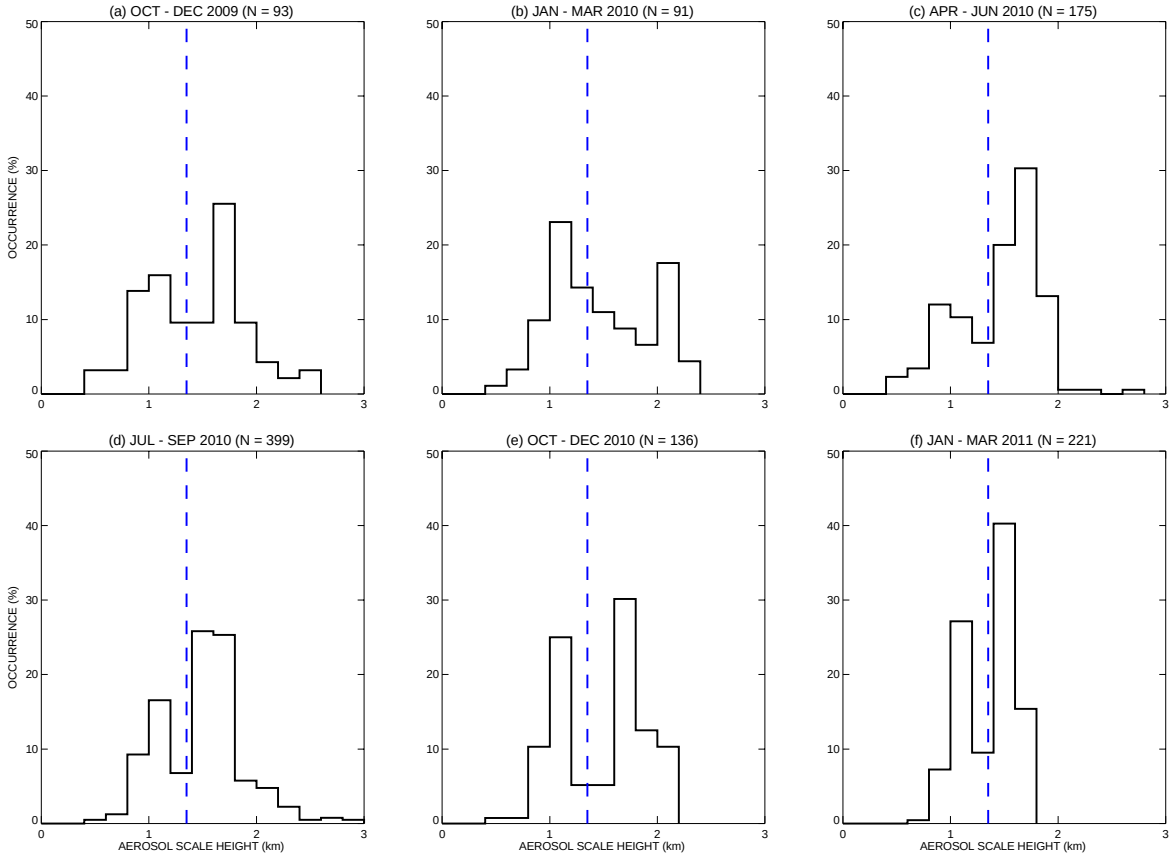
(a) OCT - DEC 2009 (N = 93)
(b) JAN - MAR 2010 (N = 91)
(c) APR - JUN 2010 (N = 175)
(d) JUL - SEP 2010 (N = 399)
(e) OCT - DEC 2010 (N = 136)
(f) JAN - MAR 2011 (N = 221)
OCCURRENCE (%)
AEROSOL SCALE HEIGHT (km)

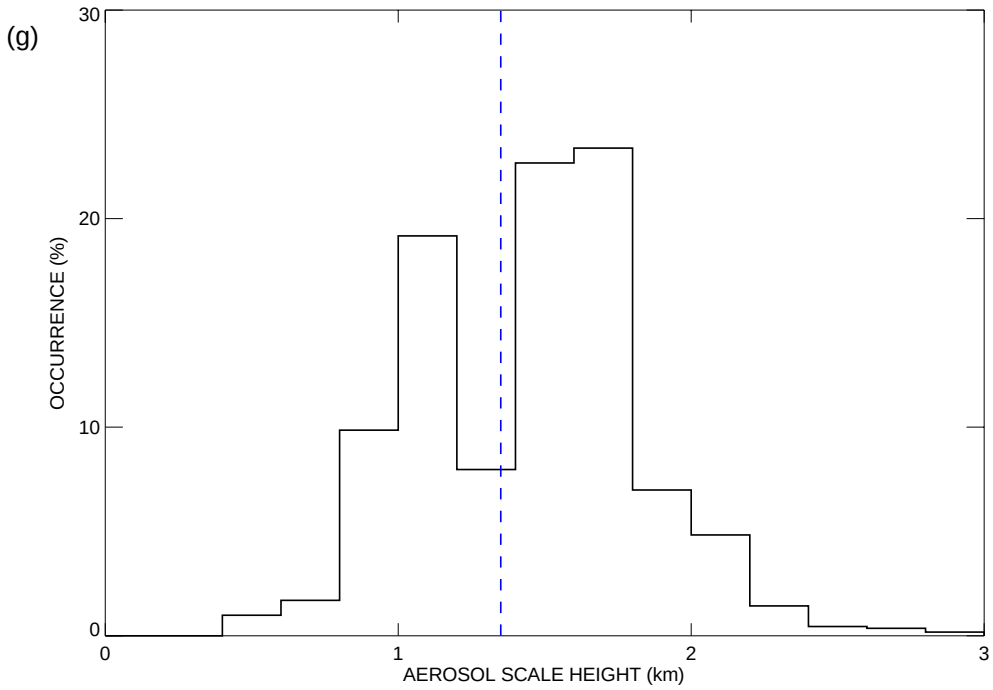
(g)
OCCURRENCE (%)
AEROSOL SCALE HEIGHT (km)

Figure 1

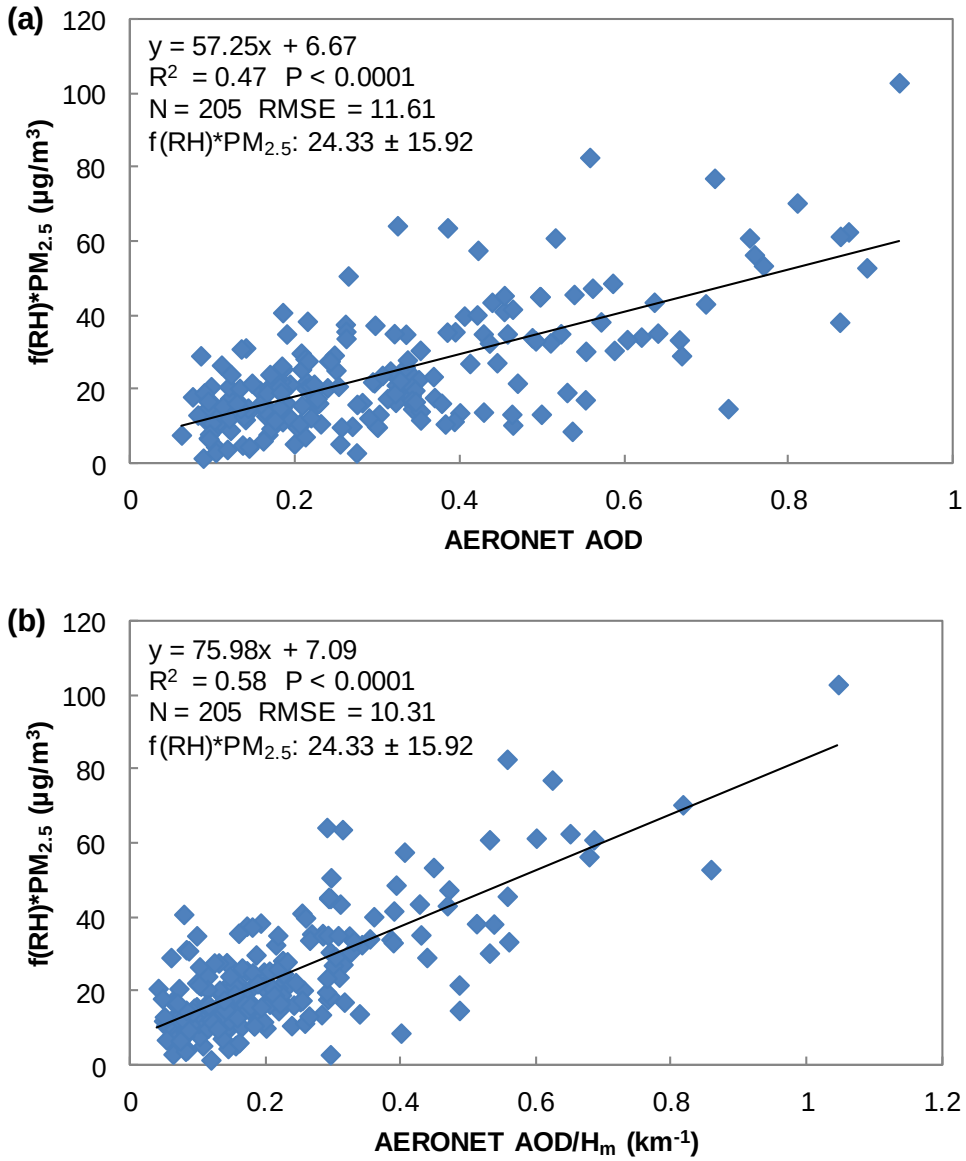
(a)
y = 57.25x + 6.67
R2 = 0.47 P < 0.0001
N = 205 RMSE = 11.61
f(RH)*PM2.5: 24.33 ± 15.92
f(RH)*PM2.5 (μg/m3)
AERONET AOD
(b)
y = 75.98x + 7.09
R2 = 0.58 P < 0.0001
N = 205 RMSE = 10.31
f(RH)*PM2.5: 24.33 ± 15.92
f(RH)*PM2.5 (μg/m3)
AERONET AOD/Hm (km-1)

Figure 2

657

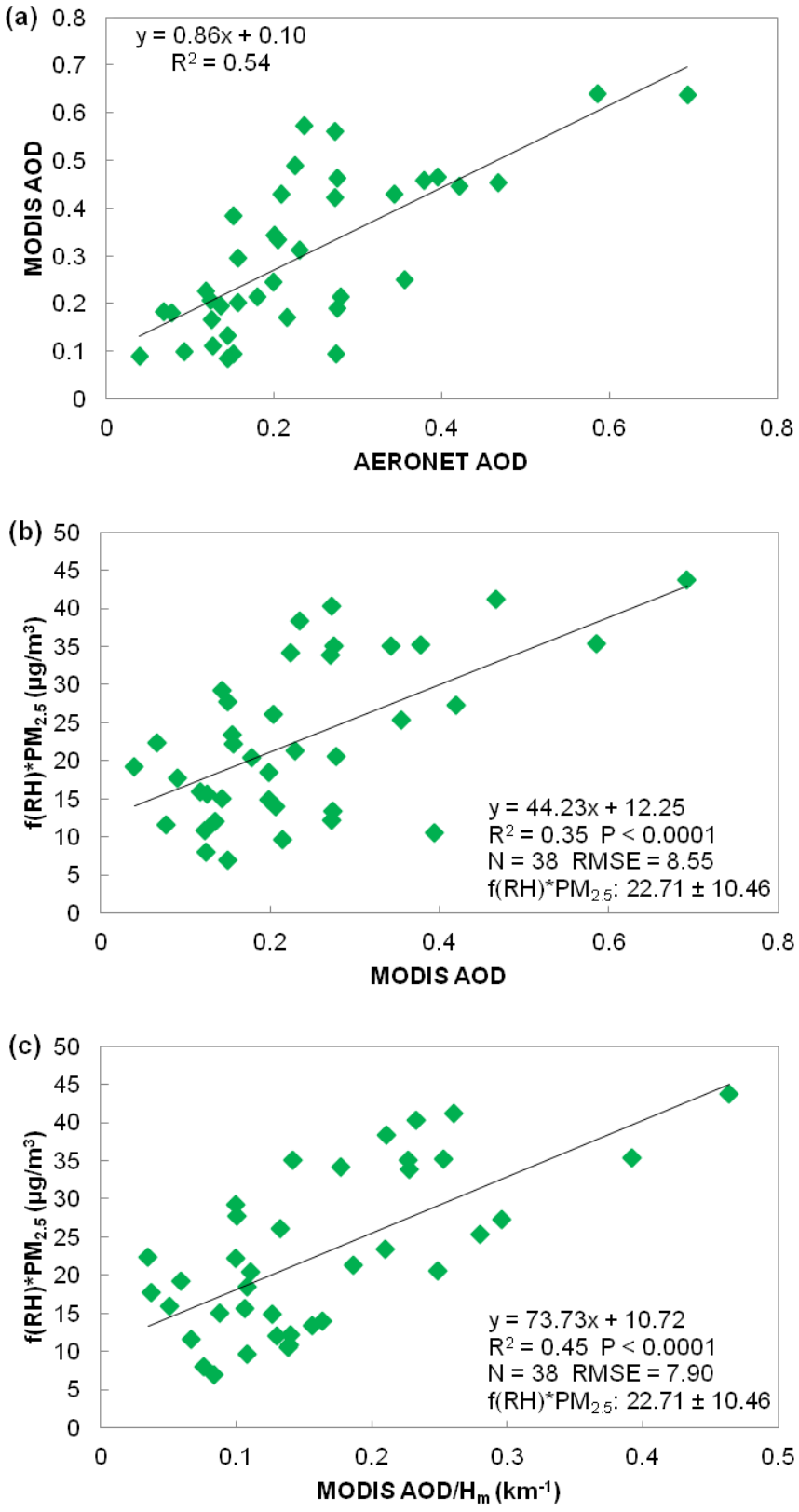
(a)
y = 0.86x + 0.10
R2 = 0.54
MODIS AOD
AERONET AOD
(b)
y = 44.23x + 12.25
R2 = 0.35 P < 0.0001
N = 38 RMSE = 8.55
f(RH)*PM2.5: 22.71 ± 10.46
f(RH)*PM2.5 (µg/m3)
MODIS AOD
(c)
y = 73.73x + 10.72
R2 = 0.45 P < 0.0001
N = 38 RMSE = 7.90
f(RH)*PM2.5: 22.71 ± 10.46
f(RH)*PM2.5 (µg/m3)
MODIS AOD/Hm (km-1)

Figure 3

658

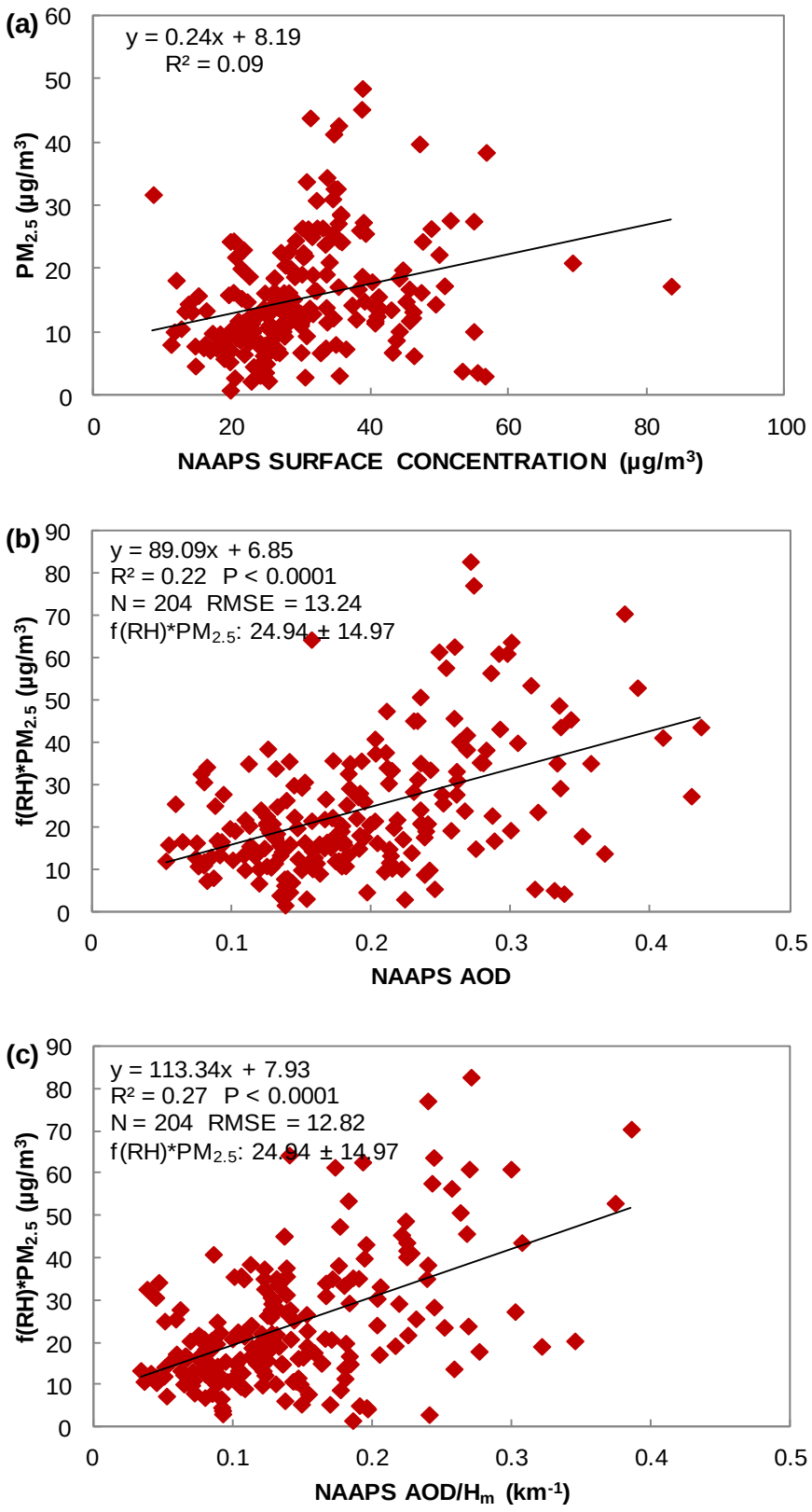
(a)
y = 0.24x + 8.19
R² = 0.09
PM2.5 (µg/m3)
NAAPS SURFACE CONCENTRATION (µg/m3)
(b)
y = 89.09x + 6.85
R² = 0.22 P < 0.0001
N = 204 RMSE = 13.24
f(RH)*PM2.5: 24.94 ± 14.97
f(RH)*PM2.5 (µg/m3)
NAAPS AOD
(c)
y = 113.34x + 7.93
R² = 0.27 P < 0.0001
N = 204 RMSE = 12.82
f(RH)*PM2.5: 24.94 ± 14.97
f(RH)*PM2.5 (µg/m3)
NAAPS AOD/Hm (km-1)

Figure 4

Table 1: Coefficients of determination (R^2) between hygroscopic-corrected $PM_{2.5}$ concentrations and MPLNET derived extinction coefficients at 100-m intervals. It should be noted that overlap corrections can be significant at heights lower than 200 m.

100 m	**200 m**	**300 m**	**400 m**	**500 m**	**600 m**	**700 m**	**800 m**	**900 m**	**1000 m**	**1100 m**	**1200 m**
0.54	0.54	0.54	0.54	0.55	0.57	0.53	0.46	0.38	0.40	0.46	0.35

664 **Table 2:** Number (N), mean, median, maximum (max) / minimum (min), and standard deviation (S.D.) for hygroscopic-corrected $PM_{2.5}$
665 measurements. Root-mean-square error (RMSE), normalized RMSE (NRMSE), and ratio of RMSE to standard deviation of observed quantities
666 (RSR) for hygroscopic-corrected $PM_{2.5}$ estimated by AOD and AOD/H_m.
667

f(RH)*PM2.5	**N**	205		38		204	
	Mean	24.33		22.71		23.94	
	Median	19.86		20.92		19.83	
	Min / Max	1.53 / 103.00		6.97 / 43.68		1.53 / 82.80	
	S.D.	15.92		10.46		14.97	
Estimated f(RH)*PM2.5		**AERONET**		**MODIS**		**NAAPS**	
		AOD	**AOD/H_m**	**AOD**	**AOD/H_m**	**AOD**	**AOD/H_m**
	RMSE	11.61	10.32	8.55	7.90	13.24	12.82
	NRMSE	0.11	0.10	0.23	0.22	0.16	0.16
	RSR	0.73	0.65	0.82	0.76	0.88	0.86

668